Clim. Past Discuss., doi:10.5194/cp-2017-2, 2017
Manuscript under review for journal Clim. Past
Published: 16 January 2017

Climate of the Past Discussions
Open Access
EGU

Multi-proxy reconstructions of precipitation field in China over the past 500 years

Feng Shi[1,2*], Sen Zhao[3,4], Zhengtang Guo[1,5,6], Hugues Goosse[2]

[1]Key Laboratory of Cenozoic Geology and Environment, Institute of Geology and Geophysics, Chinese Academy of Sciences, Beijing, 100029, China
[2]Georges Lemaître Centre for Earth and Climate Research, Earth and Life Institute, Université catholique de Louvain, Louvain-la-Neuve, 1348, Belgium
[3]Key Laboratory of Meteorological Disaster of Ministry of Education, and College of Atmospheric Science, Nanjing University of Information Science and Technology, Nanjing, 210044, China
[4]School of Ocean and Earth Sciences and Technology, University of Hawaii at Mānoa, Honolulu, HI, 96822, USA
[5]CAS Center for Excellence in Tibetan Plateau Earth Sciences, Beijing, 100101, China
[6]University of Chinese Academy of Sciences, Beijing, 100049, China

Correspondence to: Feng SHI (shifeng@mail.iggcas.ac.cn)

Abstract. The dominant modes of variability of precipitation for the whole of China over the past millennium and the mechanism governing their spatial structure remain unclear. The first reason is probably that it is difficult to reconstruct the precipitation field in western China because the published high-resolution proxy records for this region are scarce. Numerous tree-ring chronologies have recently been archived in publicly available databases through PAGES2k activities, and these provide an opportunity to refine precipitation field reconstructions for China. Based on 600 proxy records, including 491 tree-ring chronologies, 108 drought/flood indices, and a long-term instrumental precipitation record from South Korea, we revised the precipitation field reconstruction for China for the past half millennium using the optimal information extraction method. A total of 3971 of 4189 grid points in the reconstruction field passed the cross-validation process, accounting for 94.8% of the total number of grid points. The first leading mode of variability of the reconstruction shows coherent variations over most of China. The second mode, a north–south dipole in eastern China with variations of the same sign in western China and southeastern China, may be controlled by the El Niño-Southern Oscillation (ENSO) variability. The third mode, a "sandwich" triple mode in eastern China with variations of the same sign in western China and central China. Five of the six coupled ocean-atmosphere climate models (BCC-CSM1.1, CCSM4, FGOALS-s2, GISS-E2-R and MPI-ESM-P) of the Paleoclimate Modeling Intercomparison Project Phase III (PMIP3), can reproduce the south-north dipole mode of precipitation in eastern China, and its likely link with ENSO. However, there is mismatch in terms of their time development. This is consistent with an important role of the internal variability in the precipitation field changes over the past 500 years.

1 Introduction

High-resolution regional paleoclimate field reconstructions are able to accurately reproduce the fine spatiotemporal structure of regional climate change on multiple timescales for the period prior to instrumental records. Such reconstructions are an

Clim. Past Discuss., doi:10.5194/cp-2017-2, 2017
Manuscript under review for journal Clim. Past
Published: 16 January 2017

essential source of information to document the climate variability at decadal to centennial time scales and can be used to assess the ability of climate models to simulate past climate change.

In order to obtain such a reconstruction of regional paleoclimate fields, dense proxy records and an adequate reconstruction method are required. Consequently, climate field reconstructions for the past millennium have focused mainly on regions for which abundant multi-proxy records are available, including Europe (Luterbacher et al., 2004), Northern America (Cook et al., 2004) and East Asia (Shi et al., 2015a). The primary types of proxy records are tree-ring records and historical documents, mainly because of the data availability and their accurate dating, annual resolution, and demonstrable relationships with instrumental climate data (Fritts, 1976; Zhang, 1991). Other proxy records (e.g., ice core, coral, and varve sediment) have been introduced into regional climate field reconstructions (e.g., Neukom et al., 2011), but they are generally harder to use.

The targets for reconstructions are primarily on temperature variables or variables related to temperature because of their large spatial coherency. Reconstructions of the localized precipitation field or other variables related to precipitation are seldom (Cook et al., 2004; Cook et al., 2015b; Seftigen et al., 2015) because they require proxy records with more extensive distributions. In particular, the Palmer Drought Severity Index (PDSI) Atlases over the past millennium in North America (North American Drought Atlas, NADA; Cook et al., 2004), in Asia (Monsoon Asia Drought Atlas, MADA; Cook et al., 2010), in Europe (Old World Drought Atlas, OWDA; Cook et al., 2015b), and in Oceania (Australia and New Zealand summer drought atlas, ANZDA; Palmer et al., 2015) were reconstructed using the tree-ring records. All datasets are available at the website of National Oceanic and Atmospheric Administration (NOAA) (https://www.ncdc.noaa.gov/cdo/f?p=535:12:0::::P12_rec_id:179) and were widely used to identify the variability of droughts and pluvials over the past millennium (e.g., Cook et al., 2015a).

The climate field reconstruction method can be divided into the Empirical Orthogonal Function-based (EOF-based) method (Mann et al., 2009) and the point-to-point regression-based (PPR-based) method (Cook et al., 1999). The core function of the EOF-based method is to reconstruct the time coefficients of several primary EOF patterns derived from instrumental data. The left EOF patterns may retain some useful regional spatial information, which would have been partially lost in the EOF-based method. For instance, the global temperature field reconstruction using the EOF-based method (Mann et al., 2009) was not consistent with a regional temperature field reconstruction in western Qinling Mountains, China (Yang et al., 2013b). Moreover, the underlying hypothesis is that the primary spatial modes of climate change during the instrumental period also existed in the past and that the order of these principal components have not changed too much with time. The advantage of this assumption is that only a few proxy records with sparse spatial coverage are needed to reconstruct the high-resolution climate field. This approach is generally successful for temperature fields with good spatial correlation (Mann et al., 2009; Neukom et al., 2011) but is more problematic for precipitation fields because of their highly heterogeneous variability (Gómez-Navarro et al., 2015).

The PPR-based method reconstructs the climate field for individual grid points with different transform functions; e.g., the Principal Component Regression (PCR) (Cook et al., 1999), the Regularized Expectation Maximization (RegEM) regression

Clim. Past Discuss., doi:10.5194/cp-2017-2, 2017
Manuscript under review for journal Clim. Past
Published: 16 January 2017

(Shi et al., 2015a) and the optimal information extraction (OIE) method (Yang et al., 2016). In theory, the PPR-based method maximizes the retention of spatial information, but this method requires a sufficient number of suitable proxy records near the objective grid points.

The precipitation (or the variable sensitive to precipitation) field reconstruction for a large-scale region using the PPR-based method is difficult when only one type of proxy records did not cover all reconstruction areas. For example, the tree-ring based reconstruction of the MADA provides significant insights into past drought patterns in eastern Asia (Cook et al., 2010), but it performs poorly in reproducing dryness and wetness in eastern China because it only incorporates data from one short tree-ring width chronology from eastern China; consequently, it would be invalid to extrapolate objective gridded drought variability on the basis of remote tree-ring records in western China (Yang et al., 2013a).

Thus, one method to fully consider regional patterns of precipitation is to use the PPR-based method in conjunction with multi-proxy records with good spatial coverage. Among those PPR-based methods, one based on the OIE method (version 1.2) has been successfully applied recently to reconstruct the precipitation field in western Qinling Mountains, China from a multi-proxy dataset (Yang et al., 2016). This OIE method included the ensemble LOC regression (Shi et al., 2012), which was inspired from the original LOC method (Christiansen, 2011). The idea behind the ensemble LOC regression method is that the regression coefficient and error terms are random variables with normal distributions within the ranges of the linear regression and inverse regression. The LOC regression method has already been verified to efficiently retain low-frequency climate signals (Christiansen, 2011; Shi et al., 2012).

In eastern China, there are abundant historical records of precipitation variability (e.g., Hao et al., 2015). Recently, numerous tree-ring records in western China and surrounding regions have been archived in published databases (PAGES 2k Consortium, 2013; Yang et al., 2014). This presents an excellent and timely opportunity to integrate the data from tree-ring records from western China and historical records in eastern China to reconstruct the precipitation field for the whole of China. Indeed, Feng et al. (2013) reconstructed the precipitation field in East Asia using composites of multi-proxy records, which are widely used to reflect the variability in precipitation (e.g., Liu et al., 2016). However, the distribution of proxy records in western China was not sufficiently dense in that reconstruction. In addition, spatial information may have been partially lost using the EOF-based method mentioned above. This is a limitation for developing a further understanding of the dominant patterns of precipitation for the period before instrumental records and their possible driving mechanisms. In this paper, we incorporated additional tree-ring records from western China compared to previous studies and used the PPR-based framework with the OIE method to reconstruct the precipitation field for China. We present an empirical attempt to explore the dominant patterns of precipitation variability before the instrumental period and try to analyse their possible origin.

Clim. Past Discuss., doi:10.5194/cp-2017-2, 2017
Manuscript under review for journal Clim. Past
Published: 16 January 2017

2 Data and methods

To reconstruct the precipitation field, we used a gridded instrumental precipitation dataset, sensitive precipitation proxy records, and the OIE precipitation field reconstruction method. Other datasets were used to validate the reconstruction and explore possible driving mechanisms.

2.1 Instrumental data

Owing to the highly heterogeneous and localized variability in precipitation, the accuracy of regional precipitation estimates depends mainly on the spatial density of the stations (Wan et al., 2013). Thus, a dense distribution of datasets is considered a priority.

We selected a monthly gridded precipitation dataset, China's Ground Precipitation 0.5° longitude by 0.5° latitude Grid Dataset V2.0 (Zhao and Zhu, 2015), covering the period AD 1961–2010, since this dataset is calculated based on nearly all available national surface stations (n = 2474) in China. We targeted precipitation data from the warm season (May−September, MJJAS) because historical documents mainly record variations in MJJAS precipitation. The whole of China includes 4189 grid points. The calibration period was set to AD 1981–2000 and the validation period was AD 1961–1980.

Another instrumental precipitation dataset was used in this study to validate the reconstruction: The Homogenized Monthly Precipitation Dataset in China for the interval 1900–2009 (Li et al., 2012), with a 5° longitude by 5° latitude grid resolution. This dataset includes data from all available national surface stations in China before AD 1960. The MJJAS mean precipitation anomaly for China for the interval AD 1920–1960 is selected here as an independent verification data. Some unusual values were evident for the period before AD 1920, as shown in original Figure 12 of Li et al. (2012), and these are likely a result of the sparse distribution of observation points. The two datasets are both developed by, and available from, the National Meteorological Information Center, Chinese Meteorological Administration.

2.2 Tree-ring record

The use of tree-ring records has multiple advantages, including their annual resolution, easy replication, wide distribution, and significant corroboration from instrumental records. Consequently, such records are considered to be primary and practical archives for reconstructing precipitation fields in China over the past half millennium and are widely used to reconstruct regional precipitation variability in China (e.g., Yang et al., 2014).

The candidate tree-ring records are required to satisfy two conditions: 1) each record needs to at least cover the period from AD 1876 to AD 1975; 2) if raw tree-ring width measurements are available, they must be based on at least five samples for each year to ensure good replication.

To maximize the overlap lengths of the instrument data and proxy records, all tree-ring records were extrapolated to AD 2000 using the RegEM algorithm (Schneider, 2001). Here, the truncation parameters for the RegEM algorithm were set to

Clim. Past Discuss., doi:10.5194/cp-2017-2, 2017
Manuscript under review for journal Clim. Past
Published: 16 January 2017

the same values as that used by Mann et al. (2008). A total of 242 of 491 tree-ring chronologies were extrapolated. The maximum and mean extrapolation lengths of the 242 chronologies were 24 years and 10.5 years, respectively. The extrapolation bias was ignored because of the short extrapolation length.

We synthesized 491 tree-ring records from China and surrounding area, as shown in Figure 1. The tree-ring records are located mainly in India, southeastern Asia, the Tibetan Plateau, Xinjiang, Mongolia, and Japan. There are only very few tree-ring records in northeastern China and eastern China. This indicates that the currently available tree-ring records are not sufficient for reconstruction of the precipitation field in eastern China.

2.3 Dryness/Wetness index (DWI)

In eastern China, abundant records of drought and flood disasters can be found in historical documents, which provide another opportunity to reconstruct past climate (Zhang, 1991; Ge et al., 2008). A valuable example is the Yearly Charts of Dryness/Wetness in China for the Last 500-Year Period dataset (Chinese Academy of Meteorological Science, 1981). The DWI dataset, also known as the drought/flood indices (DFI), has been widely used to assess precipitation variability in eastern China (e.g., Qian et al., 2003a; Hao et al., 2015).

This DWI dataset includes data from 120 locations that are distributed mainly in eastern China and northeastern China, with a few in western China. Herein, 12 DWI are excluded because their covering too short time periods. The DWI for each year has five grade values: very wet (grade 1), wet (grade 2), normal (grade 3), dry (grade 4), and very dry (grade 5). This dataset has been extended using the annual average and standard deviation of observed rainy season precipitation (May–September, MJJAS) after AD 1980 (Zhang and Liu, 1993; Zhang et al., 2003). Thus, it does not need to be extrapolated to AD 2000. However, 51 DWI needs to be interpolated because of missing values. The RegEM method was also used to interpolate the DWI data. The maximum (mean) length for interpolation was 400 (79) years. Any interpolation bias was ignored, as the historical documentary data record a regional drought or flood event, rather than a local phenomenon, and they show good regional spatial consistency.

In total, we assembled 600 proxy records, which included 489 tree-ring width chronologies, 2 tree-ring oxygen isotope chronologies, 108 DWI, and an instrumental precipitation record from South Korea covering AD 1771–2000. Each record is required to be significantly correlated with one or more instrumental precipitation record at the 90% ($p < 0.1$) confidence level during the overlap period, based on both raw data and linearly detrended data. Moreover, previous studies have repeatedly verified a significant relationship between tree-ring precipitation reconstructions and the DWI on a regional scale (e.g., Zhang, 2010). The common period to all of the proxy records is AD 1875–1978. The number of proxy records has a visible changing point from AD 1470 to AD 1469 after extrapolation/interpolation, with a 9.50% decrease from 155 to 98. The details for each record are provided in Table s1 and Figure 1.

The two dominant modes of natural climate variability, the El Niño–Southern Oscillation (ENSO) and Pacific Decadal Oscillation (PDO), are used to explore the possible connection between our reconstruction and large-scale variability, since the two indices have already been shown to affect precipitation in China on interannual, interdecadal, and multidecadal

Clim. Past Discuss., doi:10.5194/cp-2017-2, 2017
Manuscript under review for journal Clim. Past
Published: 16 January 2017

timescales based on instrumental analysis (Huang and Wu, 1989; Ma, 2007; Qian and Zhou, 2014). Multiple ENSO and PDO reconstructions over the past millennium have been assessed in our previous work (Shi et al., 2016a). Without loss of generality, we selected three reconstructed ENSO indices (Cook et al., 2008; McGregor et al., 2010; Li et al., 2013b) and three PDO indices (D'Arrigo et al., 2001; D'Arrigo and Wilson, 2006; Shen et al., 2006) that have good performances in relationship with instrumental data. Note that three ENSO indices have a strong significant relationship during the common period AD 1650-1977 with the range of correlation coefficients [0.58, 0.66, 0.84], but three PDO indices are only very weakly related during their common period AD 1700-1979 with the range of correlation coefficients [0.03, 0.09, 0.13]. As argued recently (e.g. Newman et al., 2016), the PDO cannot be considered as a single dynamical process but results of the combined influence of remote tropical forcing and local North Pacific atmosphere–ocean interactions. This makes it a particularly challenging target for proxy-based reconstructions, explaining the poor agreement between the available series.

2.4 Climate model simulation

Six coupled climate models were used to assess whether their past1000 modeling experiments for the interval AD 850–1849 are consistent with our reconstruction. These are BCC-CSM1.1 (Wu et al., 2010), CCSM4 (Landrum et al., 2012), FGOALS-s2 (Man et al., 2014), GISS-E2-R (Schmidt et al., 2014), IPSL-CM5A-LR (Dufresne et al., 2013), and MPI-ESM-P (Jungclaus et al., 2010). The description of the six models, sponsoring institutions and main references was shown in Table s3 of Shi et al. (2015a). For details and data of the past1000 experiments, see the websites of the Paleo Modelling Intercomparison Project Phase 3 (PMIP3) and the fifth phase of the Coupled Model Intercomparison Project (CMIP5). All simulated results were interpolated to the same temporal and spatial resolution as the reconstruction in this study.

2.5 Reconstruction method

The OIE method has been successfully used to reconstruct the South Asian summer monsoon index over the past millennium (Shi et al., 2014), the Northern Hemispheric temperature over the past two millennia (Shi et al., 2015b), and the precipitation field over the past 500 years in western Qinling Mountains, China (Yang et al., 2016). The drawback of this method is an overfitting tendency. An independent test data is needed for cross validation to avoid it.

This method (version 1.2) within the PPR-based framework comprises three steps. The first step is to search for the candidate proxy records. We used the search radius method to select those following standard applications of the PPR method (Cook et al., 1999). The search radius is initially set at 450 km according to the precipitation decay correlation distance (New et al., 2000). Five is the minimum number of candidate predictors to ensure good replication of the reconstruction (Cook et al., 2013). If the number of candidate predictors is less than 5, the search radius is extended by 50 km at a time until 5 candidate predictors is found. The maximum search radius is fixed at 3500 km.

The second step is to determine the weighting for the proxy record using the correlation coefficient between the candidate proxy record and the reconstructed target. The third step is regression of the proxy record using the ensemble LOC regression method (Shi et al., 2012)

Clim. Past Discuss., doi:10.5194/cp-2017-2, 2017
Manuscript under review for journal Clim. Past
Published: 16 January 2017

Traditional accuracy and skill parameters, including the explained variance (r^2), reduction of error (RE), and coefficient of efficiency (CE) (Cook et al., 2010), were used to evaluate the reliability of the reconstructions, and the uncertainty was characterized using the standard deviation of the instrumental precipitation anomaly and the correlation coefficient between the reconstructed and instrumental precipitation anomaly (Mann et al., 2008). The significance of the correlation for the filtered time series was accessed using the effective number of degrees of freedom following Zhao et al. (2016).

The ensemble empirical mode decomposition (EEMD) method (Wu and Huang, 2009) was used to analyse the reconstructed mean MJJAS precipitation time series for eastern China, western China, and the whole of China. The eastern and western China is simply divided along - the longitude 105°. Following Mann et al. (1995), the interannual timescale was set to < 8 years. The interdecadal timescale was defined as ≥8 years and <35 years. The multidecadal timescale was defined as ≥35 years and <100 years, and the centennial scale was >100 years.

3 Results

The number of grid points as a function of the number of predictors is shown in Figure 2a. As mentioned above, the minimum number of predictors is five. The 1737 grids with five candidate proxy records account for 41.5% of the grids. The 3368 grids with ≤10 candidate proxy records account for 80.4% of the grids. The maximum number of predictors is 33. This indicates that all grid points have enough predictors. The number of grids for different search radius is shown in Figure 2b. The 1962 grids with a 450 km search radius account for 46.8% of the grids. The 3417 grids with search radii of ≤1000 km account for 81.6% of the grids. The maximum search radius is 3450 km. This implies that precipitation in most of the grid points can be reconstructed using nearby proxy records.

Figure 3 presents a summary of the reconstruction skills. Figure 3a, 3b and 3c show that the similarity in the patterns among the r^2, the RE and the CE maps, characterized by a better quality of the reconstruction in eastern China (with the exception of some regions in northeastern China) than in western China. The maximum explained variance is 0.91. The number of grids for which both the RE and CE values are greater than zero is 3971, accounting for 94.8% of the grids. This indicates that most of the grid points pass the cross-validation process. The uncertainties associated with the grids in southeastern China are greater than those for the grids in northwestern China in Fig. 3d because of large precipitation anomalies in southeastern China.

Figure 4a compares the reconstructed MJJAS mean precipitation anomalies with the instrumental MJJAS mean precipitation anomalies (Zhao and Zhu, 2015) for China for the interval AD 1961-2000. The reconstructed MJJAS mean precipitation anomalies mostly agree with the instrumental data. The correlation coefficient is 0.91 (n = 40), which is significant at the 99% confidence level. Figure 4b compares the reconstructed MJJAS mean precipitation anomalies with the instrumental MJJAS mean precipitation anomalies (Li et al., 2012) in China during AD 1900-2000. The reconstructed MJJAS mean precipitation anomaly is significantly correlated to the instrumental independent data during the interval AD 1920-1960, with a correlation coefficient of 0.57 (n = 41), also significant at the 99% confidence level. This indicates that the reconstruction passes the

Clim. Past Discuss., doi:10.5194/cp-2017-2, 2017
Manuscript under review for journal Clim. Past
Published: 16 January 2017

out-of-sample validation on the mean MJJAS precipitation anomalies for China. A part of the disagreements before AD 1919 can come actually from the uncertainties of Li et al. (2012), as specially explained in the instrumental data section.

The different components of the MJJAS precipitation anomalies for eastern China (east of 105°E), western China (west of 105°E), and whole China over the past 521 years (AD 1475-1995) are obtained using the EEMD method (Fig. 5 and Fig. s1). The amplitudes of interannual and interdecadal components in eastern China are much larger than in western China (Fig. s1), but the differences of the amplitudes of other components between eastern and western China are less clear in Fig. 5. The drought/flood changes in eastern and western China are generally consistent, but the long-term trends have opposite signs. The long-term trend in eastern China can be broadly divided into three periods: the first phase before 17th century is a partial drought condition, the second stage is wet condition from the early 17th century to the early 20th century, and then, the third stage gradually becomes a significant drought condition until now, which is consistent in previous studies (e.g., Zheng et al., 2006; Pei et al., 2015). The long-term trend in western China can be divided two stages, the first stage from the late 15th century to the early 19th century is a drought condition, and then, then second stage gradually become a significant wet condition until now. The long-term trend for whole China has similarities with the one in eastern China, but with a much weaker amplitude.

The centennial components in eastern and western China describe both a relative wet climate during the 16th century and a drought during the 17th century. The 17th century drought is also reported in previous studies (e.g., Wang et al., 2002). Moreover, the correlation coefficient of the centennial component in eastern and western China during the interval AD 1475-1849 is 0.67, but the correlation coefficient during the interval AD 1849-1995 is -0.39. This may suggest that the driver of the centennial component has changed after AD 1849.

Figure 6 shows the reconstructed 9-year running mean MJJAS precipitation anomalies for China for the interval AD 1470–2000 compared with six climate model simulations. We focus on the period during AD 1470-1849, which is a compromise between the common period of the past1000 climate model experiments (AD 850–1849) and the plausible reconstruction (AD 1470–2000). We only use the reconstruction after AD 1470 since there are no historical documents before that date. The reference period is AD 1961-1990.

Only the FGOALS-s2 results are significantly correlated with the reconstructed results during AD 1470–1849 at the 95% confidence level, but the correlation is low ($r = 0.23$). Furthermore, there is distinct shift between the mean values of the FGOALS-s2 results and the reconstruction over that period. This is related to the choice of the reference period and the increasing trend in FGOALS-s2 model since the mid-19th century in the reconstruction. All climate model simulations show low correlations with the reconstructed result. The correlation of the simulated times series is also weak between the different models. This suggests that MJJAS mean precipitation anomalies over the past 380 years in China may be largely controlled by the internal variability rather than by external forcing during the interval (AD 1470–1849). Similar conclusions were derived from the comparison of reconstructed and simulated hydroclimatic variables over the past millennium in North America (Coats et al., 2015) and in East Africa (Klein et al., 2016).

Clim. Past Discuss., doi:10.5194/cp-2017-2, 2017
Manuscript under review for journal Clim. Past
Published: 16 January 2017

Traditional EOF analysis was applied to reveal the spatial patterns in MJJAS precipitation anomalies in China over a 380-year interval (AD 1470–1849). The first four EOFs are well separated according to North et al. (1982) criteria, but the fourth EOFs only accounts for 5.1% of total variance, and its pattern is unusual in previous studies. Thus, the first three EOF patterns and their corresponding time coefficients (also known as principal components, PCs) of the MJJAS precipitation fields in China are compared with six climate model simulations in Figure 7.

The first EOF leading mode of the MJJAS precipitation field (Fig. 7a) displays a main loading in eastern China, and a general (monopole) variation over most of China, with the exception of the northeastern and western margins of the Tibetan Plateau. This mode accounts for 19.0% of the total variance, which is lower than the leading mode of temperature field (Shi et al., 2015a), but it is normal in precipitation analysis (Day et al., 2015). A main loading in eastern China also appears in the EOF1 of the reconstructed MJJAS precipitation anomalies during the interval (AD 1850–2000), the EOF1 of the reconstructed data during the interval (AD 1961–2000) and the EOF1 of the instrumental data during the same interval (AD 1961–2000). A main loading of EOF1 in eastern China is also consistent with other previous results (Wang and Zhao, 1979; Qian et al., 2003b). This is due to the large variance in eastern China, which causes the larger loads in eastern China in the other two EOFs. The EOF1 of IPSL-CM5A-LR, the EOF2 of MPI-ESM-P, and the EOF3 of CCSM4 also show a consistent variation in most of eastern China, but also some differences with the pattern deduced from the reconstruction. Furthermore. the corresponding time coefficients of model EOFs shows no obvious significant relationship with the reconstructed data (figure not shown), which was expected if natural variability is the main driver of the changes.

The second leading mode of the MJJAS precipitation field (Fig. 7b) demonstrates a south–north anomalous rainfall dipole pattern, with drying in the middle and lower reaches of the Yellow River, and increasing rainfall across and to the south of the Yangtze River. This mode accounts for 12.6% of the total variance and also appears in the EOF2 of the reconstructed MJJAS precipitation anomalies during the interval (AD 1850–2000). The South-Flood North-Drought pattern is commonly referred in previous studies from an analysis of DWI (e.g., Wang and Zhao, 1979; Qian et al., 2003b) and instrumental data (e.g., Huang et al., 1999; Yu and Zhou, 2007; Ding et al., 2008; Zhou et al., 2009). Moreover, the variations have the same sign in most of western China and southeastern China. The EOF1 from three climate models (CCSM4, FGOALS-s2, GISS-E2-R), the EOF2 from BCC-CSM1.1 model, and the EOF3 from MPI-ESM-P model reproduce a similar south–north dipole pattern in eastern China to the reconstructed results, but the specific range for each model is different. Moreover, their corresponding time coefficients show that no climate model simulation demonstrates a significant relationship with the reconstructed result (figure not shown). As mentioned for EOF1, this may be perfectly well justified if the variability of the south–north dipole pattern is dominated by internal variability.

The third leading mode illustrates a “sandwich” triple precipitation pattern with increasing rainfall in the area covering the middle and lower reaches of the Yangtze River valley, drying over southern and northern China, and variations of the same sign in most of western China and central China (Fig. 7c). This mode accounts for 8.1% of the total variance. The “sandwich” triple mode in eastern China has been reported based on the analysis of DWI (e.g., Wang and Zhao, 1979; Qian et al., 2003b) and instrumental data (e.g., Ding et al., 2008). The EOF1 from two climate models (BCC-CSM1.1 and MPI-ESM-P), the

Clim. Past Discuss., doi:10.5194/cp-2017-2, 2017
Manuscript under review for journal Clim. Past
Published: 16 January 2017

EOF2 from CCSM4 model, the EOF3 from IPSL-CM5A-LR model show similar "sandwich" triple mode to the reconstruction, and their corresponding time coefficients have again no significant relationship with the reconstructed result at the 90% confidence level (figure not shown).

4 Discussion

The first dominant mode of precipitation field with annual resolution is characterized by a monopole over all China, with the largest loading in eastern China indicating a co-variability of precipitation between monsoon and non-monsoon regions. We firstly consider the influence of the external forcing on the MJJAS precipitation anomalies variability during AD 1470-1849. The superposed epoch analysis (SEA) between the precipitation, its PC1, and 35 large eruption events during AD 1470-1849 shows that volcanic activity as one important external forcing may affect the MJJAS precipitation anomalies variability for China (Fig. 8). Nevertheless, the signals are barely significant and there are similar averaged scores before and after the volcanic eruption year, suggesting a weak influence of the eruption. The solar activity, as another potentially important external forcing, may also be part of the driving mechanism. This view is supported by the fact that the PC1 shows a weak significant relationship with solar activity index (Wang et al., 2005) ($r = 0.17$, $n = 239$) at the 95% confidence level for the interval AD 1611–1849. The correlation coefficient reaches 0.33 after the 11-year running mean filter. In summary, the influences of volcanic eruption and solar activity on PC1 are not very strong in our results. A pattern showing some similarities to the PC1 of the reconstructions appears in three climate models (Fig. 7), but the differences, in particular in western China, are too large to ensure that it has the same dynamical origin and to use model results to determine the origin of the reconstructed pattern

The second mode of annual precipitation field is the north–south dipole mode in eastern China, with variations of the same sign in most of western China and southeastern China. In fact, the north-south dipole pattern of the precipitation in eastern China was found over centennial timescale during the Medieval Warm Period and the Little Ice Age from the historical documents and speleothem records (e.g., Wang et al., 2001) and was one of dominant modes over interdecadal timescale (e.g., Ding et al., 2008).

In order to explore its possible origin, we calculated the correlation of the precipitation field with the annual mean (over the months July–June) ENSO index of McGregor et al. (2010), as shown in Figure 9. The results show a similar pattern with a north–south dipole mode in eastern China, and the precipitation anomalies in most of western China have a positive correlation with ENSO at the 90% confidence level. In addition, PC2 is significantly correlated with the ENSO index reconstruction (McGregor et al., 2010) at the 99% level ($r = 0.22$, $n = 200$) during the interval AD 1650–1849. Moreover, the other two ENSO indices (Cook et al., 2008; Li et al., 2013b) give similar correlation maps with the precipitation field (Fig. s2), but a lower correlation coefficients with PC2. This indicates that the north–south dipole in eastern China and variations of the same sign in most of western China and southeastern China are likely influenced by ENSO variability before the Industrial Revolution in our reconstruction.

Clim. Past Discuss., doi:10.5194/cp-2017-2, 2017
Manuscript under review for journal Clim. Past
Published: 16 January 2017

We calculated simulated Niño 3.4 in different seasons including the annual mean (over the months July–June), previous July to current June, previous December–January–February (DJF), current March–April–May (MAM), current June–July–August (JJA) and current MJJAS seasons. The correlation maps of five simulated MJJAS mean precipitation anomalies for China with the five-corresponding simulated annual mean Niño 3.4 indices are shown in Fig. 9. They display similar south-north dipole correlation patterns in eastern China, similar to the one from the reconstruction, for three climate models (BCC-CSM1-1, CCSM4, and MPI-ESM-P). The Niño3.4 indices in previous July to current June, previous December–January–February (DJF) and current March–April–May (MAM) seasons during AD 1470-1849 in CCSM4 model are significantly related to its PC1 at the 99% confidence level, and the correlation coefficients are 0.30, 0.30 and 0.27, respectively. The Niño3.4 indices in current June–July–August (JJA) and MJJAS seasons in FGOALS-s2 model during AD 1470-1849 are significantly related to its PC1 at the 99% confidence level, and the correlation coefficients both are 0.16. The Niño3.4 indices in previous July to current June, previous DJF, current MAM, JJA and MJJAS seasons during AD 1470-1849 in MPI-ESM-P model are significantly related to its PC3 at the 99% confidence level, the correlation coefficients are 0.23, 0.22, 0.20, 0.18, and 0.19, respectively. The EOF1 of CCSM4 model, the EOF1 of FGOALS-s2 model and the EOF3 of MPI-ESM-P model all show a similar south-north dipole mode, even the specific ranges of their spatial patterns are different. This demonstrates that ENSO has likely an imprint on the south-north dipole mode of the precipitation pattern in eastern China during AD 1470-1849 in those simulations.

Those results are consistent with previous studies based on PIMP3 model simulations suggested that La Niña (El Niño)-like conditions may explain the north-south dipole in eastern China on centennial timescale (e.g., Shi et al., 2016b) and with instrumental observations indicating that ENSO was associated with summer rainfall in eastern China (e.g., Huang and Wu, 1989; Guo et al., 2012; Schubert et al., 2016).

Based on instrumental data analysis, three general views, are used to explain the precipitation variability in eastern Asia linked to ENSO, and all of them emphasize the important bridge role of the anomalous western North Pacific anticyclone. The first one is the equatorial Rossby wave response to ENSO via the Pacific-East Asia teleconnection (Wang et al., 2000; Zhang et al., 2011; Karori et al., 2013; Feng et al., 2016). The second one is equatorial Kelvin wave response to Indian Ocean warming during El Niño decaying summer which is named “Indian Ocean capacitor effect” (Xie et al., 2009). The more recent third one is the nonlinear atmospheric interactions between ENSO and the annual cycle (Stuecker et al., 2013; Zhang et al., 2016).

We calculated the correlation map of the precipitation field with the PDO index (D'Arrigo et al., 2001) applying a 9–year running mean filter (Fig. s2). The results at the 90% confidence level show a pattern similar to EOF2 with a north–south dipole mode in eastern China. Moreover, the relationship between PDO index (D'Arrigo et al., 2001) and PC2 is strongly significant ($r = 0.41$, $n = 150$) during AD 1700–1849 at 95% confidence level after a 9-year running mean filter. However, the other two PDO indices (D'Arrigo and Wilson, 2006; Shen et al., 2006) give different correlation maps with the precipitation field (Fig. s2), and lower correlation coefficients (-0.36 and 0.07) with PC2 after a 9-year running mean filter.

Clim. Past Discuss., doi:10.5194/cp-2017-2, 2017
Manuscript under review for journal Clim. Past
Published: 16 January 2017

This indicates that the EOF2 mode is also possibly related to variations in the PDO, but the result is sensitive to the choice of the reconstructed PDO index.

Based on the instrumental data analysis, the "sandwich" triple mode in eastern China is likely associated with a meridional tripolar teleconnection in eastern Asia: the Pacific-Japan (PJ; Nitta, 1987), Pacific-East Asia (EAP, Huang and Li, 1988), or Indo-Asia-Pacific (IAP; Li et al., 2013a). The PJ/EAP/IAP teleconnection pattern can be considered as an internal mode mainly controlled by atmospheric processes (Hirota and Takahashi, 2012; Zhang and Zhou, 2015). It also can be forced by the external heating such as the anomalous convective activity in the western Pacific and tropical Indian Ocean during the El Niño decaying year (Huang and Li, 1988; Xie et al., 2009; Wu et al., 2010; Li et al., 2013a). However, there is no district evidence from the correlation maps of the reconstructed precipitation field with the ENSO and PDO indices to support this kind of mechanism for the "sandwich" pattern in this study. Alternatively, a new hypothesis was proposed recently to explain the "sandwich" triple mode through the interannual change in the strength of moisture transport from the Bay of Bengal to the Yangtze corridor across the northern Yunnan Plateau (Day et al., 2015). The increased latent heating associated with an increase in water vapor along the Yangtze corridor may generate the triple mode in eastern China and variations of the same sign in most of western China and central China.

Our results indicate thus that the south-north mode variability of precipitation anomalies in China carries very likely the fingerprint of ENSO evolution over the past 500 years, but the origin of the EOF1 and EOF3 patterns are not clearly established yet. This implies that the other factors such as North Atlantic Oscillation (NAO) (Wu et al., 2009; Zheng et al., 2016), interdecadal Pacific oscillation (IPO) (Song and Zhou, 2015), North Atlantic triple SST pattern (Ruan and Li, 2016) through the North Atlantic–Eurasia Teleconnection (AEAT) (Li et al., 2013a), the snow cover change of the Tibetan Plateau (Ding et al., 2009; Wu et al., 2012), and changes aerosol concentration (Li et al., 2016) may contribute to the reconstructed precipitation field modes during the pre-industrial period.

Some climate models (e.g., CCSM4, MPI-ESM-P) can broadly reproduce some of the dominant spatial patterns of variability of the reconstructed precipitation field for period studied. Nevertheless, the corresponding time coefficient does not match with the reconstructed series. A possible reason for this is that the precipitation changes are controlled by internal variability (e.g. related to ENSO). By constraining model result to follow the observed time series, data assimilation may then provide an interesting opportunity to analyse in more detail the mechanisms at the origin of the reconstructed changes (e.g., Widmann et al., 2010; Hakim et al., 2016).

5 Conclusions

The precipitation field for all of China was reconstructed for the past half millennium using the OIE method and additional proxy records compared to previous studies. The reconstruction shows good performance through the cross-validation process and comparison with "out-of-sample" instrumental data.

The precipitation field reconstruction reveals three leading modes for the period AD 1470–1849 before the Industrial Revolution. The first dominant mode shows consistent variation across most of China, with the exception of the northeastern and western margins of the Tibetan Plateau. This mode does not appear to be associated to the response to volcanic eruption or the solar activity. A hypothesis is that such homogenous precipitation variations in various climate regions in China have their origin in the internal variability of the system but it was not possible to determine in the present framework through which mechanism. The second mode, comprising a north–south dipole in eastern China and variations of the same sign in most of western China and southeastern China. The correlation with different reconstructions of ENSO index indicates that this dipole is likely related to variations in ENSO. The third mode is a "sandwich" triple mode in eastern China and variations of the same sign in most of western China and central China.

Moreover, the precipitation field reconstruction was used to assess the skill of PMIP3 coupled climate models. For most models, the dominant mode of variability is not characterized by relatively homogenous changes over all China, in contrast to the reconstructed fields. The correlation map between the five simulated MJJAS mean precipitation anomalies for China with the five-corresponding simulated annual mean Niño 3.4 indices shows that the ENSO has likely an imprint on the south-north dipole mode of precipitation anomaly in eastern China over the half past millennium in the simulations too. However, there is a clear model-reconstruction mismatch in reproducing the corresponding time development as they are not able to reproduce the timing of events associated to internal variability.

Acknowledgements. This work was jointly funded by the Ministry of Science and Technology of the People's Republic of China (Grant No. 2016YFA0600504), and the National Natural Science Foundation of China (Grants No. 41505081, No. 41690114, and No. 41430531). Feng Shi was supported by the "MOVE-IN Louvain" Incoming Post-doctoral Fellowship, co-funded by the Marie Curie actions of the European Commission. Hugues Goosse is Research Director with the FNRS-Fonds de la Recherche Scientifique, Belgium. We thank François Klein for his help in the processing of the data. Thanks are extended to Kevin Anchukaitis, H. P. Borgaonkar, Achim Bräuning, Brendan Buckley, Edward R. Cook, Zexin Fan, Keyan Fang, Narayan P. Gaire, Xiaohua Gou, Minhui He, Katsuhiko Kimura, Paul J. Krusic, Jiangfeng Li, Jinbao Li, Eryuan Liang, Hongbing Liu, Yu Liu, Chun Qin, Jonathan Palmer, Tatyana Papina, Jianfeng Peng, Somaru Ram, Masaki Sano, Margit Schwikowski, Xuemei Shao, Paul Sheppard, Jiangfeng Shi, Shri A.B. Sikder, Olga Solomina, Jinglin Wang, Chenxi Xu, Bao Yang, Fengmei Yang, Koh Yasue, Yujiang Yuan, Muhammad Usama Zafar, Masumi Zaiki, Qibing Zhang, Haifeng Zhu, and other paleoclimatic scientists who published the various tree-ring chronologies used in this study.

References

Chinese Academy of Meteorological Science, China Meteorological Administration (CMA): Yearly charts of dryness/wetness in China for the last 500-year period, Cartological Press, Beijing, China, 1981. (In Chinese)

Christiansen, B.: Reconstructing the NH mean temperature: Can underestimation of trends and variability be avoided? J. Climate, 24, 674-692, 2011.

Coats, S., Smerdon, J. E., Cook, B. I., and Seager, R.: Are simulated megadroughts in the North American southwest forced? J. Climate, 28, 124-142, 2015.

Cook, B. I., Ault, T. R., and Smerdon, J. E.: Unprecedented 21st century drought risk in the American Southwest and Central Plains, Sci. Adv., 1, e1400082, doi:10.1126/sciadv.1400082, 2015a.

Cook, E. R., Woodhouse, C. A., Eakin, C. M., Meko, D. M., and Stahle, D. W.: Long-term aridity changes in the western United States, Science, 306, 1015-1018, 2004.

Cook, E. R., Meko, D. M., Stahle, D. W., and Cleaveland, M. K.: Drought reconstructions for the continental United States, J. Climate, 12, 1145-1162, 1999.

Cook, E. R., D'Arrigo, R. D., Anchukaitis, K. J., and Diaz, H. F.: ENSO reconstructions from long tree-ring chronologies: Unifying the differences? In: Talk presented at a special workshop on "Reconciling ENSO Chronologies for the Past 500 Years", Moorea, 2–3 April 2008

Cook, E. R., Anchukaitis, K. J., Buckley, B. M., D'Arrigo, R., Jacoby, G. C., and Wright, W. E.: Asian monsoon failure and megadrought during the last millennium, Science, 328, 486-489, 2010.

Cook, E. R., Krusic, P. J., Anchukaitis, K. J., Buckley, B. M., Nakatsuka, T., and Sano, M.: Tree-ring reconstructed summer temperature anomalies for temperate East Asia since 800 CE, Clim. Dyn., 41, 2957-2972, 2013.

Cook, E. R., Seager, R., Kushnir, Y., Briffa, K. R., Büntgen, U., Frank, D., Krusic, P. J., Tegel, W., van der Schrier, G., Andreu-Hayles, L., Baillie, M., Baittinger, C., Bleicher, N., Bonde, N., Brown, D., Carrer, M., Cooper, R., Čufar, K., Dittmar, C., Esper, J., Griggs, C., Gunnarson, B., Günther, B., Gutierrez, E., Haneca, K., Helama, S., Herzig, F., Heussner, K.-U., Hofmann, J., Janda, P., Kontic, R., Köse, N., Kyncl, T., Levanič, T., Linderholm, H., Manning, S., Melvin, T. M., Miles, D., Neuwirth, B., Nicolussi, K., Nola, P., Panayotov, M., Popa, I., Rothe, A., Seftigen, K., Seim, A., Svarva, H., Svoboda, M., Thun, T., Timonen, M., Touchan, R., Trotsiuk, V., Trouet, V., Walder, F., Ważny, T., Wilson, R., and Zang, C.: Old World megadroughts and pluvials during the Common Era, Sci. Adv., 1, e1500561, doi:10.1126/sciadv.1500561, 2015b.

D'Arrigo, R., Villalba, R., and Wiles, G.: Tree-ring estimates of Pacific decadal climate variability, Clim. Dyn., 18, 219-224, 2001.

D'Arrigo, R., and Wilson, R.: On the Asian expression of the PDO, Int. J. Climatol., 26, 1607-1617, 2006.

Day, J. A., Fung, I. Y., and Risi, C.: Coupling of south and east Asian monsoon precipitation in July–August, J. Climate, 28, 4330-4356, 2015.

Ding, Y. H., Wang, Z. Y., and Sun, Y.: Inter-decadal variation of the summer precipitation in East China and its association with decreasing Asian summer monsoon. Part I: Observed evidences, Int. J. Climatol., 28, 1139-1161, 2008.

Ding, Y. H., Sun, Y., Wang, Z. Y., Zhu, Y. X., and Song, Y. F.: Inter-decadal variation of the summer precipitation in China and its association with decreasing Asian summer monsoon Part II: Possible causes, Int. J. Climatol., 29, 1926-1944, 2009.

Dufresne, J.-L., Foujols, M.-A., Denvil, S., Caubel, A., Marti, O., Aumont, O., Balkanski, Y., Bekki, S., Bellenger, H., and Benshila, R.: Climate change projections using the IPSL-CM5 Earth System Model: from CMIP3 to CMIP5, Clim. Dyn., 40, 2123-2165, 2013.

Feng, J., Li, J. P., Zheng, F., Xie, F., and Sun, C.: Contrasting impacts of developing phases of two types of El Niño on southern China rainfall, J. Meteor. Soc. Japan, 94, 359-370, 2016.

Feng, S., Hu, Q., Wu, Q. R., and Mann, M. E.: A gridded reconstruction of warm season precipitation for Asia spanning the past half millennium, J. Climate, 26, 2192-2204, 2013.

Fritts, H.: Tree rings and climate, Academic Press London, 1976.

Ge, Q. S., Zheng, J. Y., Tian, Y. Y., Wu, W. X., Fang, X. Q., and Wang, W.-C.: Coherence of climatic reconstruction from historical documents in China by different studies, Int. J. Climatol., 28, 1007-1024, 2008.

Gómez-Navarro, J. J., Werner, J., Wagner, S., Luterbacher, J., and Zorita, E.: Establishing the skill of climate field reconstruction techniques for precipitation with pseudoproxy experiments, Clim. Dyn., 45, 1395-1413, 2015.

Guo, Y., Li, J. P., and Li, Y.: A time-scale decomposition approach to statistically downscale summer rainfall over North China, J. Climate, 25, 572-591, 2012.

Hakim, G. J., Emile-Geay, J., Steig, E. J., Noone, D., Anderson, D. M., Tardif, R., Steiger, N., and Perkins, W. A.: The last millennium climate reanalysis project: Framework and first results, J. Geophys. Res. [Atmos.], 121, 6745-6764, 2016.

Hirota, N., and Takahashi, M.: A tripolar pattern as an internal mode of the East Asian summer monsoon, Clim. Dyn., 39, 2219-2238, 2012.

Huang, R. H., and Li, W. J.: Influence of heat source anomaly over the western tropical Pacific on the subtropical high over East Asia during summer and its physical mechanism, Chin. J. Atmos. Sci., 107-117, 1988.

Huang, R. H., and Wu, Y. F.: The influence of ENSO on the summer climate change in China and its mechanism, Adv. Atmos. Sci., 6, 21-32, 1989.

Huang, R. H., Xu, Y. H., and Zhou, L. T.: The interdecadal variation of summer precipitations in China and the drought trend in North China, Plateau Meteor., 18, 465-476, 1999. (In Chinese)

Jungclaus, J. H., Lorenz, S. J., Timmreck, C., Reick, C. H., Brovkin, V., Six, K., Segschneider, J., Giorgetta, M. A., Crowley, T. J., Pongratz, J., Krivova, N. A., Vieira, L. E., Solanki, S. K., Klocke, D., Botzet, M., Esch, M., Gayler, V., Haak, H., Raddatz, T. J., Roeckner, E., Schnur, R., Widmann, H., Claussen, M., Stevens, B., and Marotzke, J.: Climate and carbon-cycle variability over the last millennium, Clim Past, 6, 723-737, 2010.

Karori, M. A., Li, J., and Jin, F.-F.: The asymmetric influence of the two types of El Niño and La Niña on summer rainfall over Southeast China, J. Climate, 26, 4567-4582, 2013.

Klein, F., Goosse, H., Graham, N. E., and Verschuren, D.: Comparison of simulated and reconstructed variations in East African hydroclimate over the last millennium, Clim Past, 12, 1499-1518, 2016.

Landrum, L., Otto-Bliesner, B. L., Wahl, E. R., Conley, A., Lawrence, P. J., Rosenbloom, N., and Teng, H.: Last millennium climate and its variability in CCSM4, J. Climate, 26, 1085-1111, 2012.

Li, J. P., Ren, R. C., Qi, Y. Q., Wang, F. M., Lu, R. Y., Zhang, P. Q., Jiang, Z. H., Duan, W. S., Yu, F., and Yang, Y. Z.: Progress in air-land-sea interactions in Asia and their role in global and Asian climate change, Chin. J. Atmos. Sci., 37, 518-538, 2013a. (In Chinese)

Li, J. B., Xie, S.-P., Cook, E. R., Morales, M. S., Christie, D. A., Johnson, N. C., Chen, F. H., D/'Arrigo, R., Fowler, A. M., Gou, X. H., and Fang, K. Y.: El Niño modulations over the past seven centuries, Nat. Clim. Change, 3, 822-826, 2013b.

Li, Q. X., Peng, J. D., and Shen, Y.: Development of China homogenized monthly precipitation dataset during 1900-2009, J. Geog. Sci., 22, 579-593, 2012.

Li, Z. Q., Lau, W. M., Ramanathan, V., Wu, G. X., Ding, Y. H., Manoj, M., Liu, J., Qian, Y., Li, J., Zhou, T. J., Fan, J., Rosenfeld, D., Ming, Y., Wang, Y., Huang, J., Wang, B., Xu, X., Lee, S-S., Cribb, M., Zhang, F., Yang, X., Takemura, T., Wang, K., Xia, X., Yin, Y., Zhang, H., Guo, J., Zhai, P. M., Sugimoto, N., Babu S. S., and Brasseur, G. P.: Aerosol and monsoon climate interactions over Asia, Rev. Geophys., 54, doi:10.1002/2015RG000500, 2016.

Liu, F., Chai, J., Wang, B., Liu, J., Zhang, X., and Wang, Z. Y.: Global monsoon precipitation responses to large volcanic eruptions, Sci. Rep., 6, 24331, doi:10.1038/srep24331, 2016.

Luterbacher, J., Dietrich, D., Xoplaki, E., Grosjean, M., and Wanner, H.: European seasonal and annual temperature variability, trends, and extremes since 1500, Science, 303, 1499-1503, 2004.

Ma, Z.: The interdecadal trend and shift of dry/wet over the central part of North China and their relationship to the Pacific Decadal Oscillation (PDO), Chin. Sci. Bull., 52, 2130-2139, 2007.

Man, W. M., Zhou, T. J., and Jungclaus, J. H.: Effects of large volcanic eruptions on global summer climate and East Asian monsoon changes during the Last millennium: Analysis of MPI-ESM simulations, J. Climate, 27, 7394-7409, 2014.

Clim. Past Discuss., doi:10.5194/cp-2017-2, 2017
Manuscript under review for journal Clim. Past
Published: 16 January 2017

Mann, M. E., Park, J., and Bradley, R.: Global interdecadal and century-scale climate oscillations during the past five centuries, Nature, 378, 266-270, 1995.

Mann, M. E., Zhang, Z. H., Hughes, M. K., Bradley, R. S., Miller, S. K., Rutherford, S., and Ni, F. B.: Proxy-based reconstructions of hemispheric and global surface temperature variations over the past two millennia, Proc. Nat. Acad. Sci. U.S.A., 105, 13252-13257, 2008.

Mann, M. E., Zhang, Z. H., Rutherford, S., Bradley, R. S., Hughes, M. K., Shindell, D., Ammann, C., Faluvegi, G., and Ni, F. B.: Global Signatures and Dynamical Origins of the Little Ice Age and Medieval Climate Anomaly, Science, 326, 1256-1260, 2009.

McGregor, S., Timmermann, A., and Timm, O.: A unified proxy for ENSO and PDO variability since 1650, Clim Past, 6, 1-17, 2010.

Neukom, R., Luterbacher, J., Villalba, R., Kuttel, M., Frank, D., Jones, P. D., Grosjean, M., Wanner, H., Aravena, J. C., Black, D. E., Christie, D. A., D'Arrigo, R., Lara, A., Morales, M., Soliz-Gamboa, C., Srur, A., Urrutia, R., and von Gunten, L.: Multiproxy summer and winter surface air temperature field reconstructions for southern South America covering the past centuries, Clim. Dyn., 37, 35-51, 2011.

New, M., Hulme, M., and Jones, P.: Representing twentieth-century space-time climate variability. Part II: Development of 1901-96 monthly grids of terrestrial surface climate, J. Climate, 13, 2217-2238, 2000.

Newman, M., Alexander, M. A., Ault, T. R., Cobb, K. M., Deser, C., Di Lorenzo, E., Mantua, N. J., Miller, A. J., Minobe, S., and Nakamura, H.: The Pacific decadal oscillation, revisited, J. Climate, 29, 4399-4427, 2016.

Nitta, T.: Convective activities in the tropical western Pacific and their impact on the Northern Hemisphere summer circulation, J. Meteor. Soc. Japan., 65, 373-390, 1987.

North, G. R., Bell, T. L., Cahalan, R. F., and Moeng, F. J.: Sampling errors in the estimation of empirical orthogonal functions, Mon. Weather Rev., 110, 699-706, 1982.

PAGES 2k Consortium (Ahmed, M., Anchukaitis, K. J., Asrat, A., Borgaonkar, H. P., Braida, M., Buckley, B. M., Büntgen, U. l. f., Chase, B. M., Christie, D. A., Cook, E. R., Curran, M. A. J., Diaz, H. F., Esper, J., Fan, Z. X., Gaire, N. P., Ge, Q. S., Gergis, J., González-Rouco, J. F., Goosse, H., Grab, S. W., Graham, N., Graham, Rochelle., Grosjean, Martin., Hanhijärvi, S. T., Kaufman, D. S., Kiefer, T., Kimura, K., Korhola, A. A., Krusic, P. J., Lara, A., Lézine, A.-M., Ljungqvist, F. C., Lorrey, A. M., Luterbacher, J., Masson-Delmotte, V., McCarroll, D., McConnell, J. R., McKay, N. P., Morales, M. S., Moy, A. D., Mulvaney, R., Mundo, I. A., Nakatsuka, T., Nash, D. J., Neukom, R., Nicholson, S. E., Oerter, H., Palmer, J. G., Phipps, S. J., Prieto, M. R., Rivera, A., Sano, M., Severi, M., Shanahan, T. M., Shao, X. M., Shi, F., Sigl, M., Smerdon, J. E., Solomina, O. N., Steig, E. J., Stenni, B., Thamban, M., Trouet, V., Turney, C. S. M., Umer, M., van Ommen, T., Verschuren, D., Viau, A. E., Villalba, R., Vinther, B. M., von Gunten, L., Wagner, S., Wahl, E. R., Wanner, H., Werner, J. P., White, J. W. C.,

Yasue, K., and Zorita, E.): Continental-scale temperature variability during the past two millennia, Nat. Geosci., 6, 339-346, 2013.

Palmer, J. G., Cook, E. R., Turney, C. S., Allen, K., Fenwick, P., Cook, B. I., O'Donnell, A., Lough, J., Grierson, P., and Baker, P.: Drought variability in the eastern Australia and New Zealand summer drought atlas (ANZDA, CE 1500–2012) modulated by the Interdecadal Pacific Oscillation, Environ. Res. Lett., 10, 124002, doi:10.1088/1748-9326/10/12/124002, 2015.

Pei, L., Yan, Z. W., and Hui, Y.: Multidecadal variability of dry/wet patterns in eastern China and their relationship with the Pacific Decadal Oscillation in the last 413 years, Chin. Sci. Bull., 60, 97-108, 2015.

Qian, C., and Zhou, T. J.: Multidecadal variability of North China aridity and its relationship to PDO during 1900–2010, J. Climate, 27, 1210-1222, 2014.

Qian, W. H., Hu, Q., Zhu, Y., and Lee, D. K.: Centennial-scale dry-wet variations in East Asia, Clim. Dyn., 21, 77-89, 2003a.

Qian, W. H., Chen, D., Zhu, Y., and Shen, H. Y.: Temporal and spatial variability of dryness/wetness in China during the last 530 years, Theor. Appl. Climatol., 76, 13-29, 2003b.

Ruan, C. Q., and Li, J. P.: An improvement in a time-scale decomposition statistical downscaling prediction model for summer rainfall over North China. Chinese Journal of Atmospheric Sciences, Chin. J. Atmos. Sci., 40, 215-226, 2016.

Schmidt, G. A., Kelley, M., Nazarenko, L., Ruedy, R., Russell, G. L., Aleinov, I., Bauer, M., Bauer, S. E., Bhat, M. K., and Bleck, R.: Configuration and assessment of the GISS ModelE2 contributions to the CMIP5 archive, J. Adv. Model Earth Sy., 6, 141-184, 2014.

Schneider, T.: Analysis of incomplete climate data: Estimation of mean values and covariance matrices and imputation of missing values, J. Climate, 14, 853-871, 2001.

Schubert, S. D., Stewart, R. E., Wang, H., Barlow, M., Berbery, E. H., Cai, W., Hoerling, M. P., Kanikicharla, K. K., Koster, R. D., and Lyon, B.: Global meteorological drought: A synthesis of current understanding with a focus on SST drivers of precipitation deficits, J. Climate, 29, 3989-4019, 2016.

Seftigen, K., Björklund, J., Cook, E., and Linderholm, H.: A tree-ring field reconstruction of Fennoscandian summer hydroclimate variability for the last millennium, Clim. Dyn., 44, 3141-3154, 2015.

Shen, C., Wang, W. C., Gong, W., and Hao, Z.: A Pacific Decadal Oscillation record since 1470 AD reconstructed from proxy data of summer rainfall over eastern China, Geophys. Res. Lett., 33, L03702, doi:10.1029/2005GL024804, 2006.

Shi, F., Yang, B., Charpentier Ljungqvist, F., and Fengmei, Y.: Multi-proxy reconstruction of Arctic summer temperatures over the past 1400 years, Clim. Res., 54, 113-128, 2012.

Shi, F., Li, J., and Wilson, R. J. S.: A tree-ring reconstruction of the South Asian summer monsoon index over the past millennium, Sci. Rep., 4, doi:10.1038/srep06739, 2014.

Shi, F., Ge, Q. S., Yang, B., Li, J. P., Yang, F. M., Ljungqvist, F. C., Solomina, O., Nakatsuka, T., Wang, N. L., Zhao, S., Xu, C. X., Fang, K. Y., Sano, M., Chu, G. Q., Fan, Z. X., Narayan, P. G., and Muhammad, U. Z.: A multi-proxy reconstruction of spatial and temporal variations in Asian summer temperatures over the last millennium, Clim. Change 131, 663-676, 2015a.

Shi, F., Yang, B., Feng, J., Li, J. P., Yang, F. M., and Guo, Z. T.: Reconstruction of the Northern Hemisphere annual temperature change over the common era derived from tree rings, Quat. Sci., 35, 1051-1063, 2015b. (In Chinese)

Shi, F., Fang, K. Y., Xu, C. X., Guo, Z. T., and Borgaonkar H. P.: Interannual to centennial variability of the South Asian summer monsoon over the past millennium, Clim. Dyn., doi:10.1007/s00382-016-3493-9, 2016a.

Shi, J., Yan, Q., Jiang, D. B., Min, J., and Jiang, Y.: Precipitation variation over eastern China and arid central Asia during the past millennium and its possible mechanism: Perspectives from PMIP3 experiments, J. Geophys. Res. [Atmos.], 121, 11989-12004, 2016b.

Song, F., and Zhou, T. J.: The crucial role of internal variability in modulating the decadal variation of the East Asian summer monsoon–ENSO relationship during the twentieth century, J. Climate, 28, 7093-7107, 2015.

Stuecker, M. F., Timmermann, A., Jin, F.-F., McGregor, S., and Ren, H.-L.: A combination mode of the annual cycle and the El Nino/Southern Oscillation, Nature Geosci, 6, 540-544, 2013.

Wan, H., Zhang, X. B., Zwiers, F. W., and Shiogama, H.: Effect of data coverage on the estimation of mean and variability of precipitation at global and regional scales, J. Geophys. Res. [Atmos.], 118, 534-546, 2013.

Wang, B., Wu, R. G., and Fu, X. H.: Pacific–east Asian teleconnection: How does ENSO affect east Asian climate? J. Climate, 13, 1517-1536, 2000.

Wang, S. W., Gong, D. Y., and Zhu, J. H.: Twentieth-century climatic warming in China in the context of the Holocene, Holocene, 11, 313-321, 2001.

Wang, S. W., Cai, J. N., Mu, Q. Z., Xie, Z. H., and Dong, W. J.: Climate change of annual precipitations in western China, J. Nat. Resour., 17, 415-422, 2002.

Wang, S. W., and Zhao, Z. C.: An analyses of historical data of droughts and floods in last 500 years in China, Acta Geographica Sinica, 34, 329–341, 1979. (In Chinese)

Wang, Y. M., Lean, J. L., and Sheeley, N. R.: Modeling the sun's magnetic field and irradiance since 1713, Astrophys. J., 625, 522-538, 2005.

Widmann, M., Goosse, H., van der Schrier, G., Schnur, R., and Barkmeijer, J.: Using data assimilation to study extratropical Northern Hemisphere climate over the last millennium, Clim Past, 6, 627-644, 2010.

Wu, B., Li, T., and Zhou, T. J.: Relative contributions of the Indian Ocean and local SST anomalies to the maintenance of the Western North Pacific anomalous anticyclone during the El Niño decaying summer, J. Climate, 23, 2974-2986, 2010.

Wu, T. W., Yu, R. C., Zhang, F., Wang, Z. Z., Dong, M., Wang, L. N., Jin, X., Chen, D. L., and Li, L.: The Beijing Climate Center atmospheric general circulation model: description and its performance for the present-day climate, Clim. Dyn., 34, 123-147, 2010.

Wu, Z. H., and Huang, N.: Ensemble empirical mode decomposition: a noise assisted data analysis method, Adv. Adapt. Data Anal., 1, 1-41, 2009.

Wu, Z. W., Wang, B., Li, J. P., and Jin, F. F.: An empirical seasonal prediction model of the East Asian summer monsoon using ENSO and NAO, J. Geophys. Res. [Atmos.], 114, doi:10.1029/2009JD011733, 2009.

Wu, Z. W, Li, J. P., Jiang, Z. H., and Ma, T. T.: Modulation of the Tibetan Plateau snow cover on the ENSO teleconnections: From the East Asian summer monsoon perspective, J. Climate, 25, 2481-2489, 2012.

Xie, S.-P., Hu, K., Hafner, J., Tokinaga, H., Du, Y., Huang, G., and Sampe, T.: Indian Ocean capacitor effect on Indo-western Pacific climate during the summer following El Niño, J. Climate, 22, 730-747, 2009.

Yang, B., Qin, C., Wang, J. L., He, M. H., Melvin, T. M., Osborn, T. J., and Briffa, K. R.: A 3,500-year tree-ring record of annual precipitation on the northeastern Tibetan Plateau, Proceedings of the National Academy of Sciences, 111, 2903-2908, 2014.

Yang, F. M., Shi, F., Kang, S. Y., Wang, S. G., Xiao, Z. N., Nakatsuka, T., and Shi, J.: Comparison of the dryness/wetness index in China with the Monsoon Asia Drought Atlas, Theor. Appl. Climatol., 114, 553-566, 2013a.

Yang, F. M., Wang, N. A., Shi, F., Ljungqvist, F. C., Wang, S. G., Fan, Z. X., and Lu, J. W.: Multi-proxy temperature reconstruction from the West Qinling Mountains, China, for the past 500 years, Plos One, 8, e57638, doi:10.1371/journal.pone.0057638, 2013b.

Yang, F. M., Wang, N. A., Shi, F., Ljungqvist, F. C., Zhao, S., and Liu, T.: The spatial distribution of precipitation over the West Qinling region, China, AD 1470–2000, Palaeogeogr. Palaeoclimatol. Palaeoecol., 443, 278-285, 2016.

Yu, R. C., and Zhou, T. J.: Seasonality and three-dimensional structure of interdecadal change in the East Asian monsoon, J. Climate, 20, 5344-5355, 2007.

Zhang, D.: Historical records of climate change in China, Quat. Sci. Rev., 10, 551-554, 1991.

Zhang, D., and Liu, C.: Continuation (1980-1992) of the yearly charts of dryness/wetness in China for the last 500 years period, Meteorol. Mon., 19, 41-45, 1993.

Zhang, D., Li, X., and Liang, Y.: Continuation (1992-2000) of the yearly charts of dryness/wetness in China for the last 500 years period, J. Appl. Meteor. Sci., 14, 379-384, 2003.

Zhang, D.: Test of calibration on the paleoclimatic proxy data by using Chinese historical records, Advances in Climate Change Research, 6, 70-72, 2010.

Zhang, L. X., and Zhou, T. J.: Drought over East Asia: A review, J. Climate, 28, 3375-3399, 2015.

Zhang, W., Jin, F.-F., Li, J., and Ren, H.-L.: Contrasting impacts of two-type El Niño over the western North Pacific during boreal autumn, Journal of the meteorological Society of Japan, 89, 563-569, 2011.

Zhang, W. J., Jin, F. F., Stuecker, M. F., Wittenberg, A. T., Timmermann, A., Ren, H. L., Kug, J. S., Cai, W. J., and Cane, M.: Unraveling El Niño's impact on the East Asian Monsoon and Yangtze River summer flooding, Geophys. Res. Lett., 43, 11375-11382, 2016.

Zhao, S., Li, J. P., and Sun, C.: Decadal variability in the occurrence of wintertime haze in central eastern China tied to the Pacific Decadal Oscillation, Sci. Rep., 6, doi:10.1038/srep27424, 2016.

Zhao, Y. F., and Zhu, J.: Assessing quality of grid daily precipitation datasets in China in recent 50 years, Plateau Meteor., 34, 50-58, 2015. (In Chinese)

Zheng, F., Li, J., Li, Y., Zhao, S., and Deng, D.: Influence of the summer NAO on the spring-NAO-based predictability of the East Asian summer monsoon, J. Appl. Meteorol. Climatol., 2016.

Zheng, J., Wang, W., Ge, Q., Man, Z., and Zhang, P.: Precipitation variability and extreme events in eastern China during the past 1500 years, Terr. Atmos. Ocean Sci., 17, 579-592, 2006.

Zhou, T. J., Gong, D., Li, J., and Li, B.: Detecting and understanding the multi-decadal variability of the East Asian summer monsoon recent progress and state of affairs, Meteorol. Z., 18, 455-467, 2009.

Clim. Past Discuss., doi:10.5194/cp-2017-2, 2017
Manuscript under review for journal Clim. Past
Published: 16 January 2017

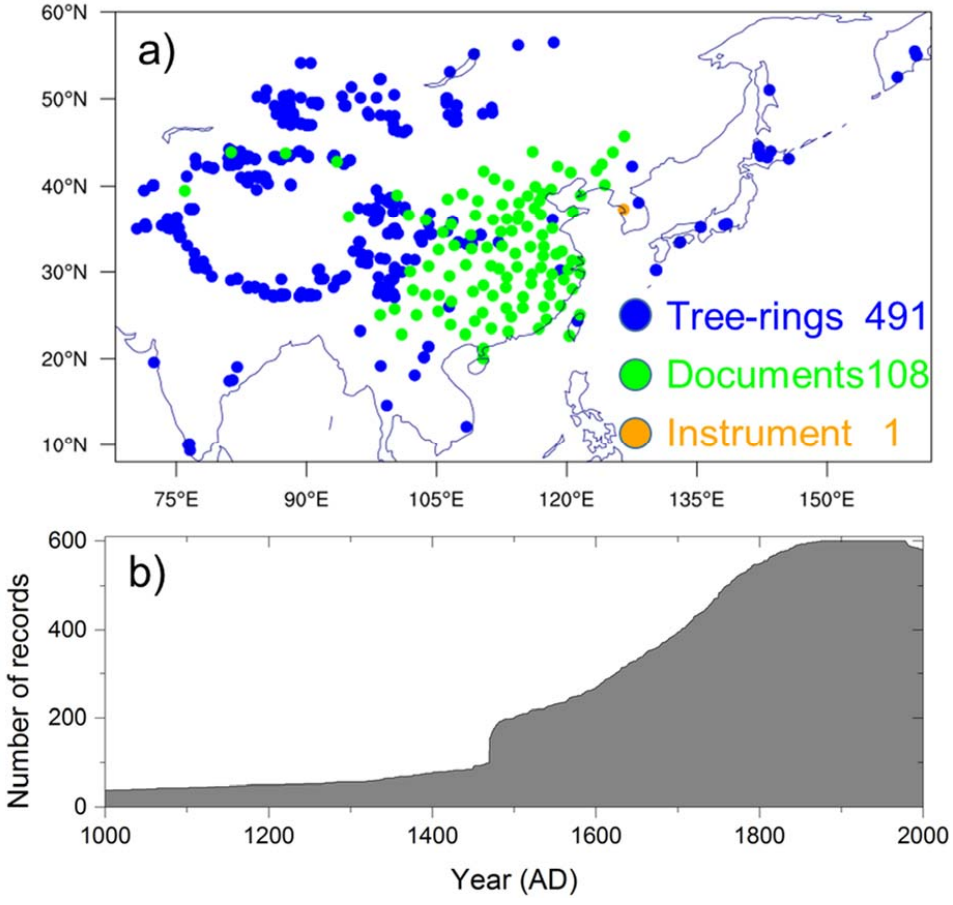

Figure 1: Map showing the locations of proxy records (a) and plot of the first year covered by each proxy record (b).

Clim. Past Discuss., doi:10.5194/cp-2017-2, 2017
Manuscript under review for journal Clim. Past
Published: 16 January 2017

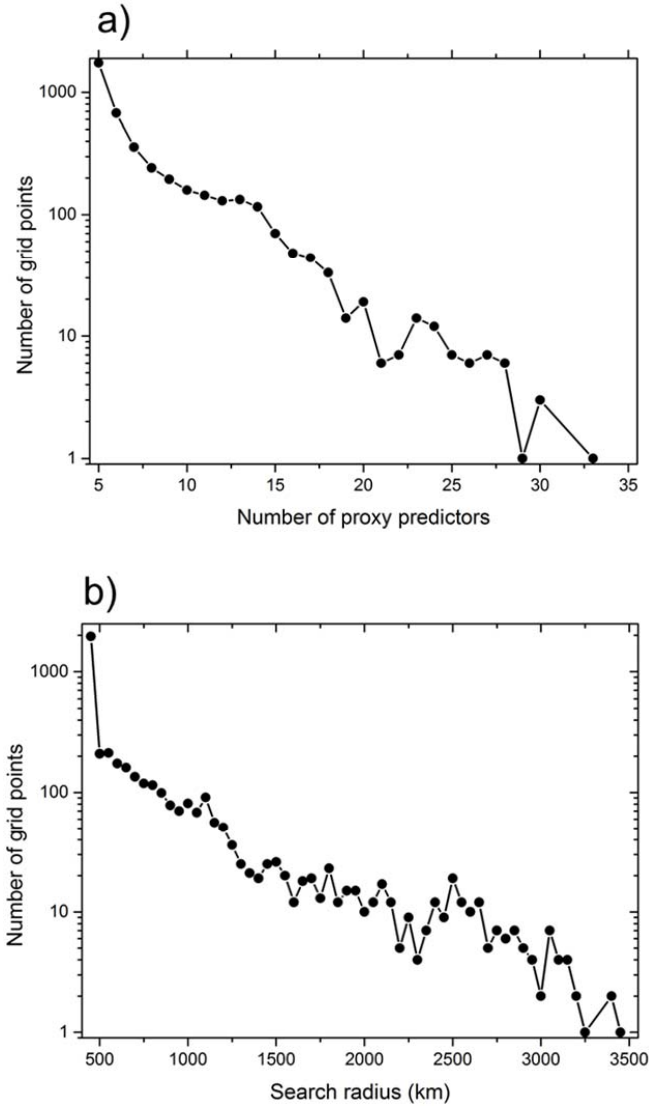

Figure 2: The number of grid points as a function of a given number of proxy predictors (a) or a given search radius (b).

Clim. Past Discuss., doi:10.5194/cp-2017-2, 2017
Manuscript under review for journal Clim. Past
Published: 16 January 2017

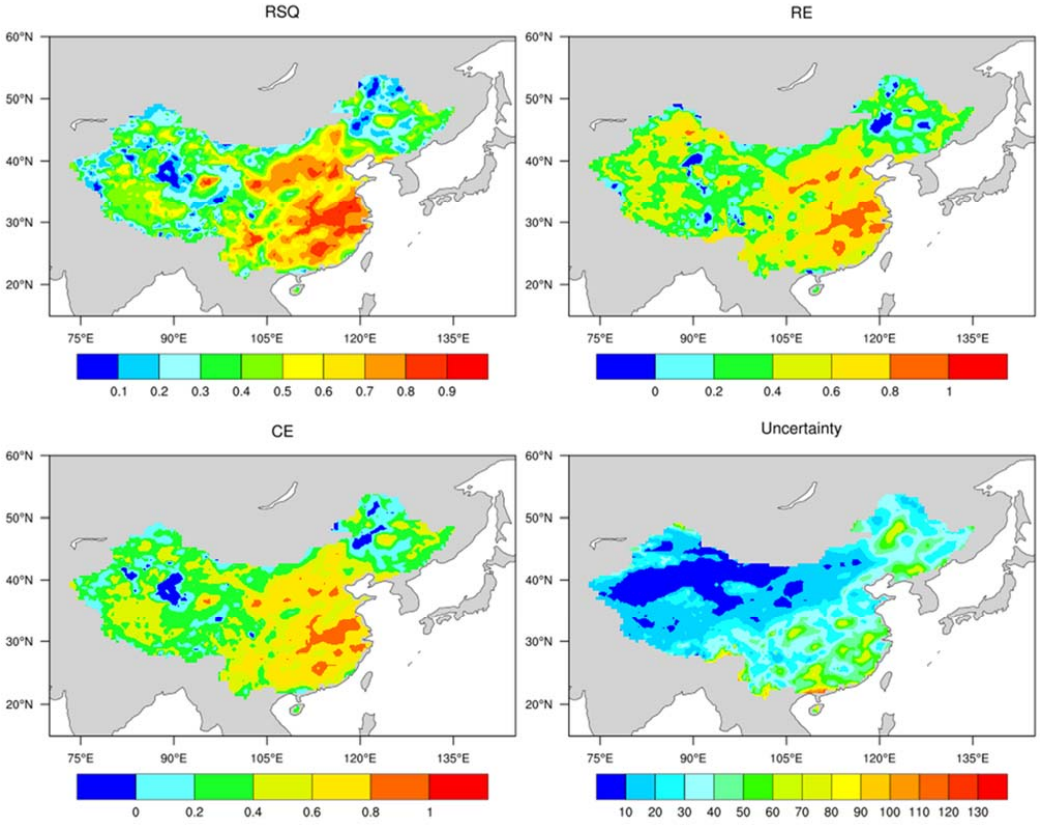

Figure 3: Skills of the reconstructed MJJAS mean precipitation anomalies in China for the 1961–1980 verification period and the 1981–2000 calibration period.

Clim. Past Discuss., doi:10.5194/cp-2017-2, 2017
Manuscript under review for journal Clim. Past
Published: 16 January 2017

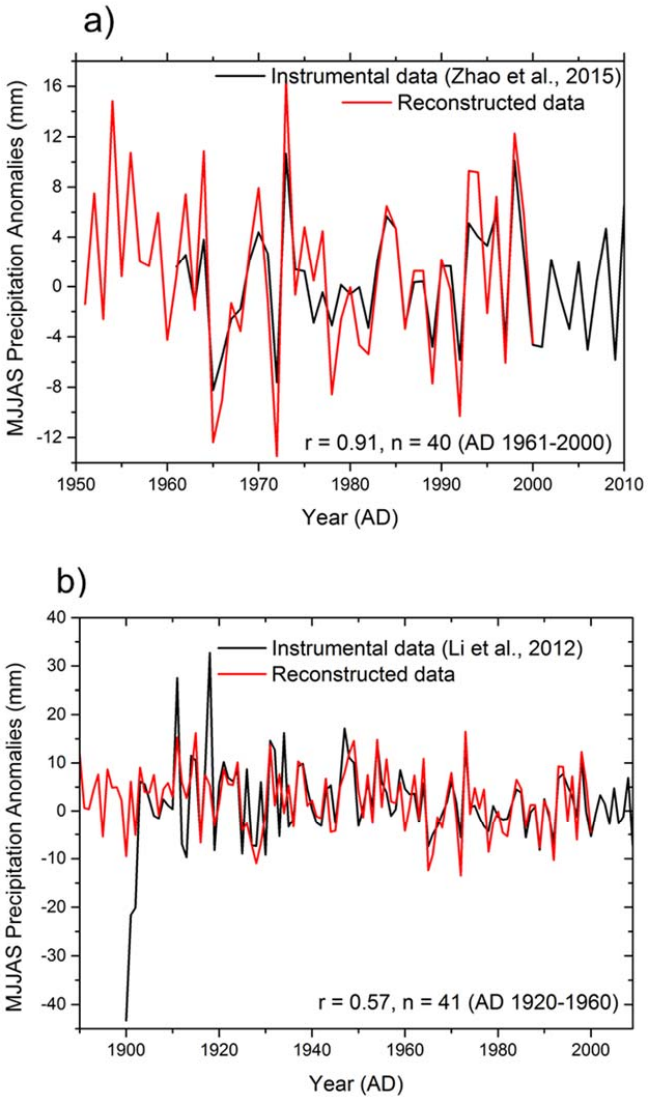

Figure 4: Comparison of the reconstructed and instrumental MJJAS mean precipitation anomalies for China. (a) instrumental data (Zhao et al., 2015); (b) instrumental data (Li et al., 2012).

Clim. Past Discuss., doi:10.5194/cp-2017-2, 2017
Manuscript under review for journal Clim. Past
Published: 16 January 2017

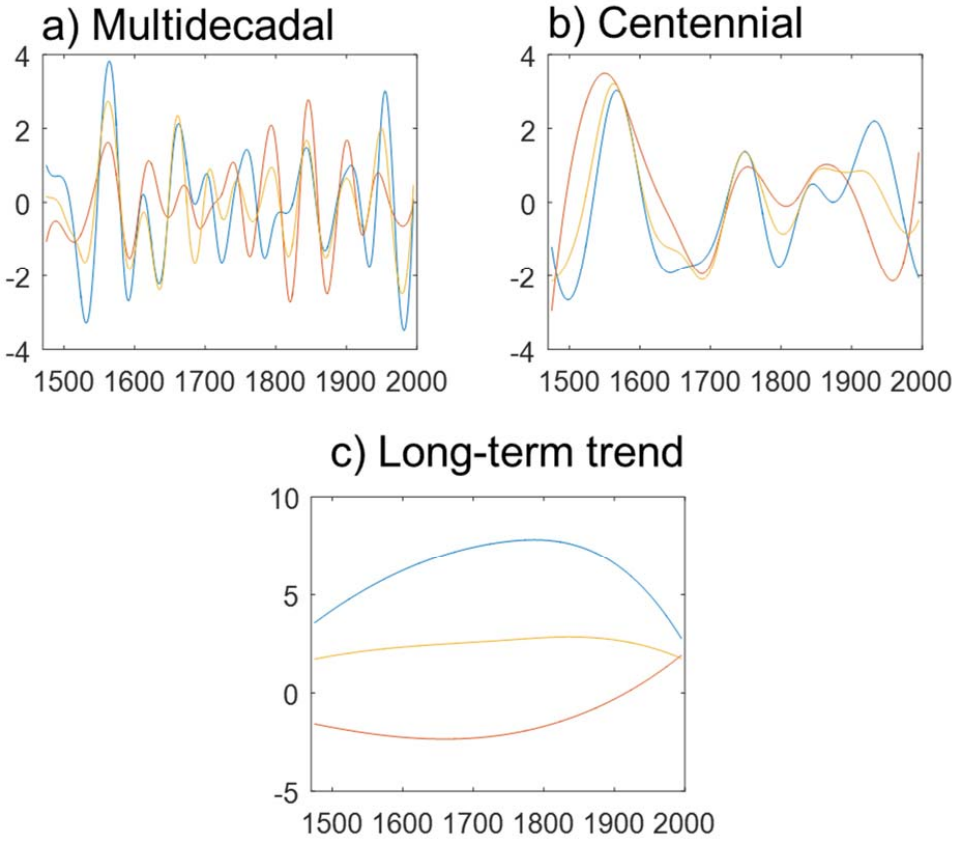

Figure 5: The intrinsic mode functions (IMFs) of the mean MJJAS precipitation anomalies for eastern China (blue line), western China (red line), and whole China (yellow line), over the past 521 years (AD 1475-1995) using the Ensemble Empirical mode decomposition (EEMD) method, including the multidecadal (a), centennial (b), and long-term trend (c) components.

Clim. Past Discuss., doi:10.5194/cp-2017-2, 2017
Manuscript under review for journal Clim. Past
Published: 16 January 2017

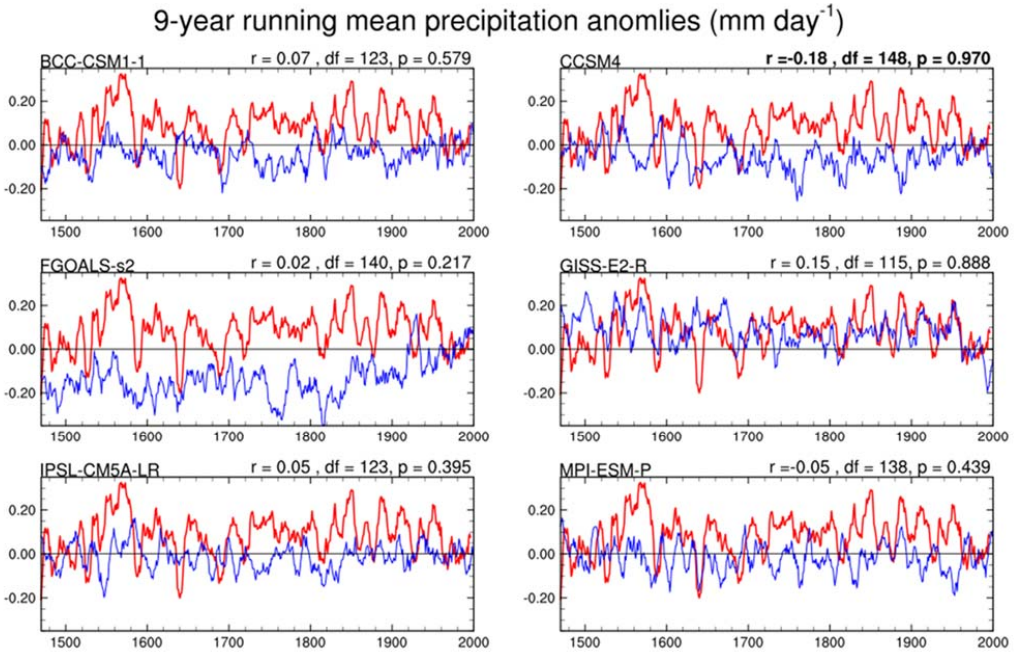

Figure 6: Comparison of the 9-year running mean reconstructed and six simulated MJJAS mean precipitation anomalies for China during the interval AD 1470–2000.

Clim. Past Discuss., doi:10.5194/cp-2017-2, 2017
Manuscript under review for journal Clim. Past
Published: 16 January 2017

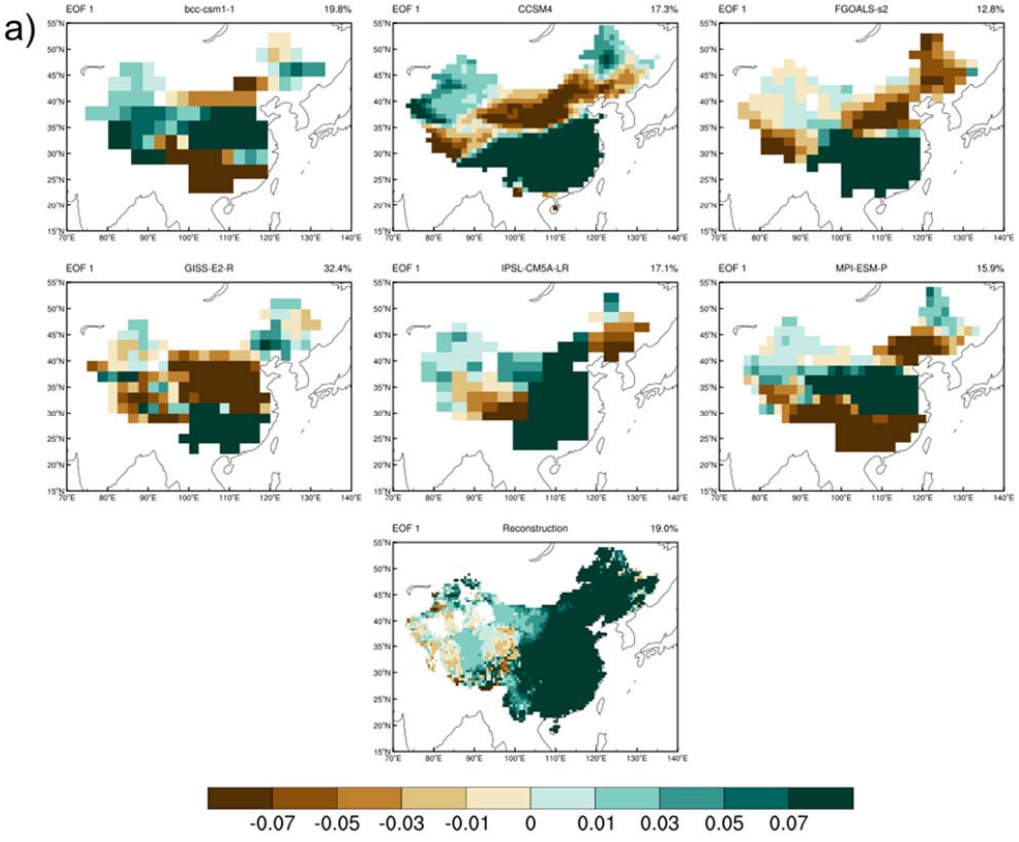

Figure 7a: Empirical orthogonal function (EOF) 1 of the MJJAS mean precipitation anomalies for China during the interval AD 1470–1849.

Clim. Past Discuss., doi:10.5194/cp-2017-2, 2017
Manuscript under review for journal Clim. Past
Published: 16 January 2017

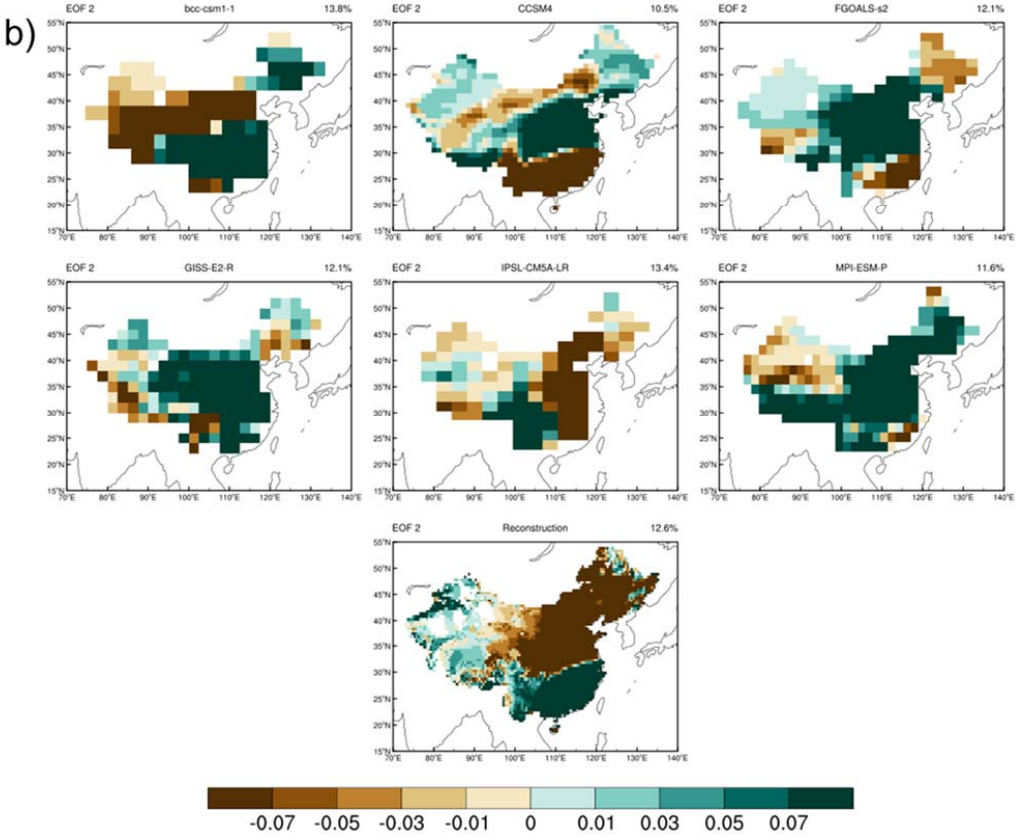

Figure 7b: Empirical orthogonal function (EOF) 2 of the MJJAS mean precipitation anomalies for China during the interval AD 1470–1849.

Clim. Past Discuss., doi:10.5194/cp-2017-2, 2017
Manuscript under review for journal Clim. Past
Published: 16 January 2017

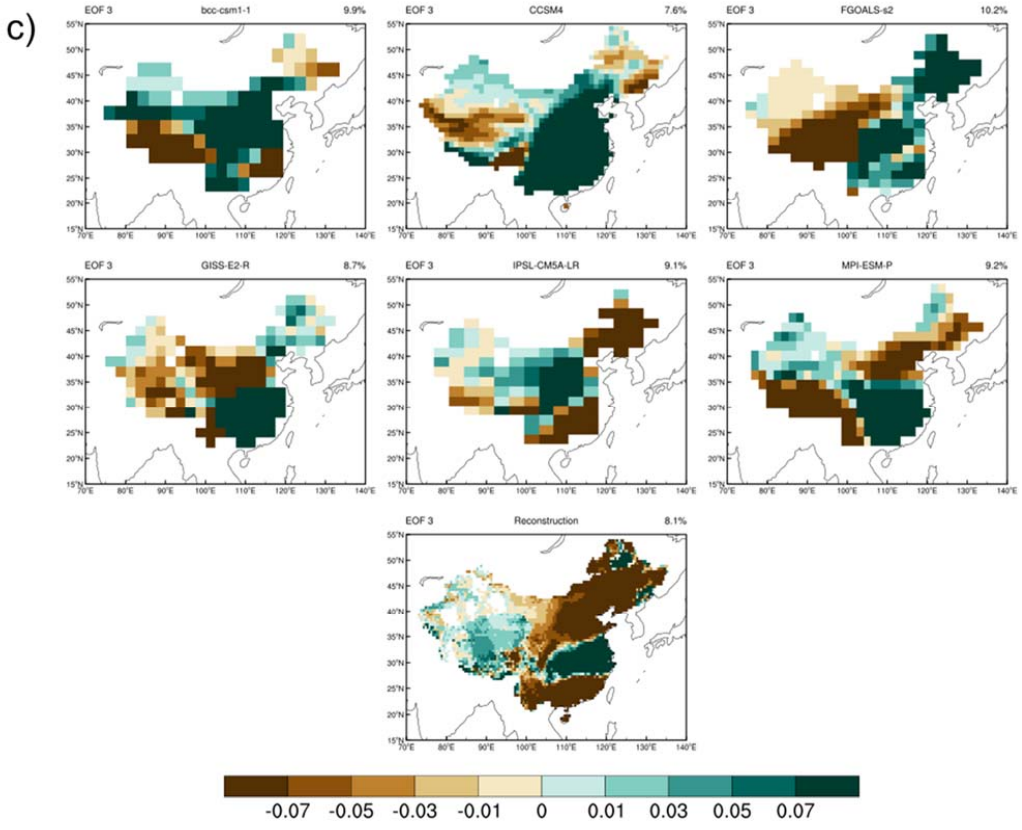

Figure 7c: Empirical orthogonal function (EOF) 3 of the MJJAS mean precipitation anomalies for China during the interval AD 1470–1849.

Clim. Past Discuss., doi:10.5194/cp-2017-2, 2017
Manuscript under review for journal Clim. Past
Published: 16 January 2017

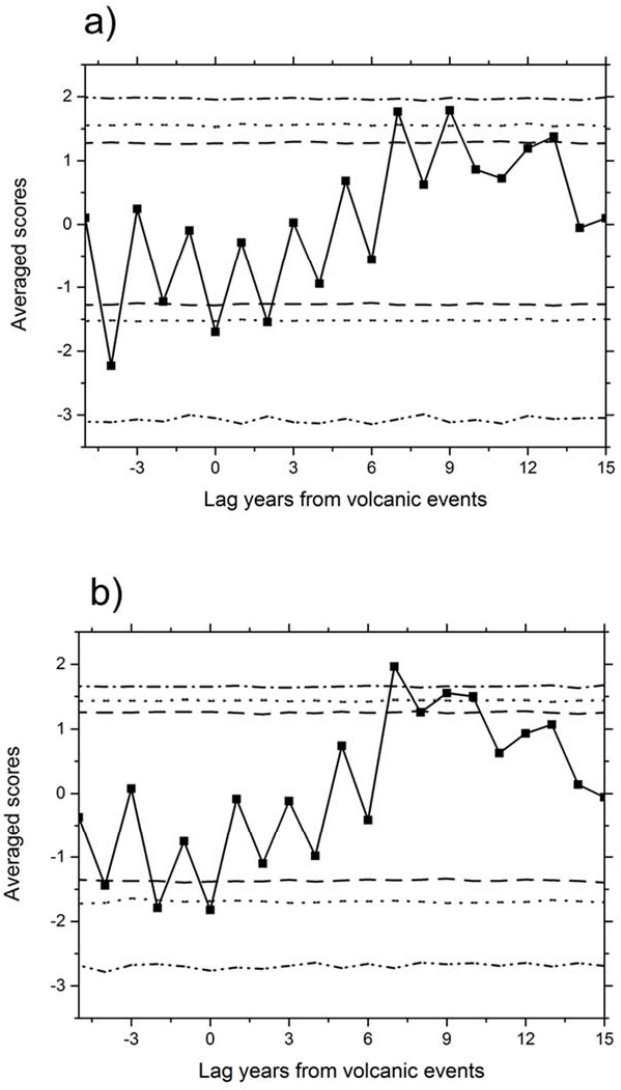

Figure 8: Superposed Epoch Analysis results applied to the precipitation (a) and its PC1 (b) response to 35 large volcanic events (Sigl et al., 2015) with 90%, 95% and 99% confidence limits of the mean given as dashed, dotted, and dashed-dotted lines, respectively.

Clim. Past Discuss., doi:10.5194/cp-2017-2, 2017
Manuscript under review for journal Clim. Past
Published: 16 January 2017

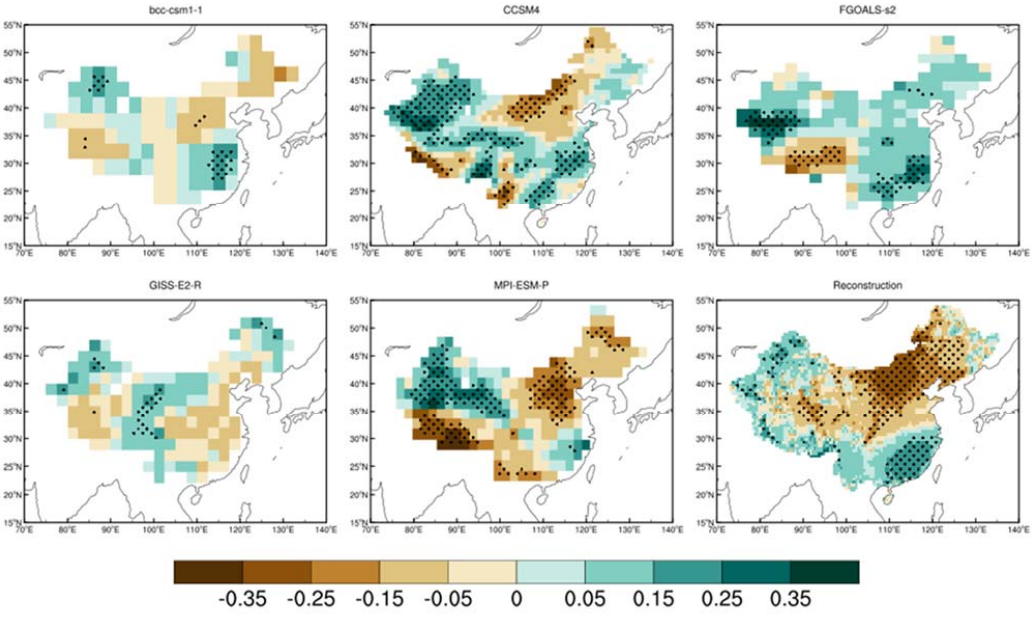

Figure 9: Correlation maps of five simulated and a reconstructed MJJAS mean precipitation anomalies for China with the five-corresponding simulated annual mean Niño 3.4 indices and a reconstructed annual mean ENSO index (McGregor et al., 2010).